AIAA Aviation
16-20 June 2014, Atlanta, GA
32nd AIAA Applied Aerodynamics Conference

A continuous adjoint-based approach for the optimization of wing flapping

Min Xu*, Mingjun Wei†
New Mexico State University, Las Cruces, NM 88003

The study of flapping-wing aerodynamics is a problem with very large control space. Adjoint-based approach, by solving an inverse problem, can be used here as an efficient tool for optimization and physical understanding. However, the adjoint equation is typically formulated in a fixed domain. The moving boundary or morphing domain brings in an inconsistency in the definition of arbitrary perturbation at the boundary, which then proposes a new challenge if the control parameters happen to be also at the boundary. An unsteady mapping function, as a usual remedy for such problems, would make the whole formulation too complex to be feasible. Instead, we use non-cylindrical calculus to re-define the perturbation and solve the inconsistency caused by moving/morphing solid boundaries. The approach is first validated for a simple two dimensional test case of a plate plunging in an incoming flow. Then, we apply the approach to reduce the drag of a rigid flapping plate by optimize the phase delay between the plunging and pitching motion as a constant (single parameter) and as a time-varying function (large number of parameters). The extension to three dimensional cases is successfully validated by applying on an oscillatory sphere with incoming flow.

I. Introduction

The mechanism of flapping-wing dynamics provides an efficient way to generate necessary lift and thrust and has been the most common way of flying adopted by birds and insects. In comparison with other flying mechanism used by nature's flyers and artificial machines, flapping shows many attractive characteristics such as agility, hovering capability, efficiency in low Reynolds number, etc. Though some degree of understanding may be revealed by ways such as carefully designed numerical simulations [1–4], the problem's large parametric space prevents a usual parametric study by checking them one by one and the optimization of all the parameters becomes impossible to reach directly from such case study.

To solve this problem, one may have to reduce the complexity of the problem and the size of parametric space. Based on a quasi-steady model with 11 control parameters, Berman & Wang were able to use a hybrid algorithm of genetic method and simplex method to minimize the power consumption of insect flights [5]. Ghommem *et al.* used unsteady vortex-lattice method and a deterministic global optimization algorithm for the optimization of flapping wings in forward flight with active morphing, where only 4 to 8 parameters were considered [6]. Milano & Gharib applied genetic algorithm in an experimental setting to maximize the average lift from flapping flat plates by limiting the control parameters to only 4 [7]. There have also been efforts to use gradient-based method for optimization. Tuncer & Kaya [8] and Culbreth *et al.* [9] used an gradient-based method to optimize the flapping-wing motion for better thrust and efficiency. They used direct numerical simulation for each set of control parameters and then calculated the gradient of the cost function to the change of parameters directly by finite difference. Since each parameters were evaluated individually and required their own simulation, the process became very expensive, and the former work used only 4 parameters and the latter used 1 to 11 parameters.

Different from above works, Nadarajah & Jameson [10] used an adjoint-based method to obtain the gradient information for the shape optimization of a plunging airfoil. By its nature, the adjoint approach can obtain the gradient information simultaneously for arbitrary number of input parameters (e.g. large

*PhD Candidate, Department of Mechanical and Aerospace Engineering, Student Member AIAA
†Associate Professor, Department of Mechanical and Aerospace Engineering, Senior Member AIAA

number of control points for the definition of different airfoil shapes) by one single computation in adjoint space. Consequently, the total computational cost to obtain the sensitivity of the cost function to all control parameters is independent of the number of control parameters. Thus, it makes adjoint-based method suitable for the sensitivity analysis and optimization for problems with large input space but small output space. It was also our inspiration of applying adjoint-based method on the flapping-wing problem. However, we noticed that, in the work of Nadarajah & Jameson [10], an unsteady mapping function is used to transfer the physical domain with moving boundary to a computational domain with fixed boundary, so that, traditional adjoint-based method for fixed domain can be applied. The mapping function has increased the complexity of the formulation considerably, though Nadarajah & Jameson only optimized the steady part (i.e. the shape) of the unsteady mapping function. A complete optimization of flapping wings involve trajectory and deformation as time-dependent functions, and the control changes both the boundary shape and velocity dynamically. For such cases, applying unsteady mapping function becomes too complex to be feasible. Instead, we apply here the idea of non-cylindrical calculus [11, 12] to derive the adjoint equations directly in a morphing domain and optimize the moving boundary in its original space (without mapping function).

Based on the order of discretization and adjoint-formulation, there are normally two types of adjoint approaches: continuous approach [13, 14] and discrete approach [15, 16]. There are pros and cons in both approaches [17, 18]. We pick the continuous approach here for its simplicity and clarity in the governing equation for adjoint space, which has math terms showing certain "physical meaning" such as the generation, convection and dissipation of the adjoint field [19]. The continuous approach also provides the flexibility of choosing different numerical implementations.

The rest of the paper is arranged in the following manner. The governing equations are given in § II, and numerical simulation details are described in § III. Then, there are validation and application of our algorithm in § IV. The final conclusions are discussed in § V.

II. Derivation of the Adjoint Equations

The basic derivation of continuous adjoint equation is similar to the one used in the work of Bewley *et al.* [13] and our earlier work [14], though those earlier work dealt only with problems with fixed domain. The inclusion of non-cylindrical calculus to formulate adjoint equation in a morphing domain has been suggested by Moubachir & and Zolèsio [11] and Protas & Liao [12]. We have extended the idea and implemented in Navier-Stokes equations with preliminary results reported in an earlier work [20]. Some derivations from the earlier work [20] is reviewed in this section for the completeness of the paper.

II.A. Governing equation and cost function

First, we consider a scenario where a plate is plunging and/or pitching with prescribed velocity $V(t)$. We choose the prescribed velocity as control, $V(t) = \phi(t)$, and use a simple objective/cost function, for demonstration, which is to minimize the overall difference between velocity $\mathbf{u}$ at a downstream region Ω_o and the target velocity $\mathbf{u}_0$ for a time duration $(0, T)$. The cost function can be described mathematically as

$$\mathcal{J} = \int_0^T \int_{\Omega_o} |\mathbf{u} - \mathbf{u}_0|^2 d\mathbf{x}dt. \tag{1}$$

With the above cost function $\mathcal{J}$ defined, its sensitivity to the control ϕ can be achieved from the perturbed function $\mathcal{J}'$ subjected to arbitrary perturbation ϕ':

$$\mathcal{J}' \equiv \lim_{\varepsilon \to 0} \frac{\mathcal{J}(\phi + \varepsilon\phi') - \mathcal{J}(\phi)}{\varepsilon}. \tag{2}$$

When optimization is considered, the gradient $g(\phi)$ can be derived from above sensitivity analysis to update the control variables iteratively as

$$\phi^{\text{new}} = \phi^{\text{old}} - \alpha g(\phi^{\text{old}}). \tag{3}$$

The cost of the optimization process is mainly determined by the convergence speed as for a typical gradient-based method. Conjugate gradient method and other methods to accelerate the convergence are normally involved.

The current physical problem is described by incompressible Navier-Stokes equations

$$\begin{aligned} \mathcal{N}(\mathbf{q}) &= \mathbf{F} \qquad in\ \ \Omega, \\ u_i &= V_i \qquad on\ \ \mathcal{S}. \end{aligned} \tag{4}$$

where Ω represents the fluid domain, $\mathcal{S}$ denotes the solid boundary, the primary variable $\mathbf{q} = [p\ \mathbf{u}]^T$,

$$\mathcal{N}(\mathbf{q}) = \begin{bmatrix} \dfrac{\partial u_j}{\partial x_j} \\ \dfrac{\partial u_i}{\partial t} + \dfrac{\partial u_j u_i}{\partial x_j} - \nu \dfrac{\partial^2 u_i}{\partial x_j^2} + \dfrac{\partial p}{\partial x_i} \end{bmatrix}, \qquad \mathbf{F} = 0. \tag{5}$$

II.B. Noncylindrical calculus

As shown above, the gradient information comes from the perturbation to control ϕ, which is defined by Fréchet differential:

$$\mathbf{q}' \equiv \lim_{\varepsilon \to 0} \frac{\mathbf{q}(t, \phi + \varepsilon\phi', \mathbf{x}) - \mathbf{q}(t, \phi, \mathbf{x})}{\varepsilon}. \tag{6}$$

For problems with moving/morphing boundaries and the control on the boundaries, this definition proposes ambiguity on those locations. For example, to be consistent with the governing equation of fluid mechanics, the derivative is usually defined in a Eulerian point of view. However, the status of Eulerian points may change between on and off the boundary when the boundary is moving. To make the problem more serious, for the moment when a Eulerian point moving to/from a solid region, it is not defined by above fluid equations. On the other hand, if the perturbation is defined in a Lagrangian point of view, a bridge is needed to link all the value back to the Eulerian framework where all variables and equations are defined.

To solve this problem, one can use a unsteady mapping function to transfer the whole domain and problem to a computational domain with fixed boundaries [10,17]. However, such an approach often results in complexity. In the recent work of Nadarajah & Jameson [10], they applied the mapping method only to Euler equation and optimize only the shape of a rigid airfoil in plunging motion. In other words, the optimization is only about the steady portion (shape without morphing) but not the unsteady portion (trajectory or shape deformation) of the whole unsteady mapping function. Otherwise, their unsteady mapping approach would be very complex as it is demonstrated by Protas & Liao [12] using a simple 1D unsteady problem controlled by heat equation.

Instead, we adopted the approach of noncylindrical calculus [11,12], which will handle and only handle the change on the domain boundary. In fact, one of the reason for the complexity brought in by using mapping function is that the mapping of interior points is entirely unnecessary for the optimization of boundary motion and deformation. We have approved the equivalence of these two approaches (mapping function and noncylindrical calculus), however, the proof is too lengthy to be included here.

To introduce noncylindrical calculus, we first define a flowmap $\mathcal{T}$ which describes the time evolution of domain Ω with the same control ϕ:

$$\mathcal{T}(t, \tau, \phi) : \Omega(t, \phi) \to \Omega(t + \tau, \phi), \tag{7}$$

where it requires boundary-to-boundary mapping and no topological change is allowed. Then, a flowmap velocity $\mathbb{V}$ is defined by its derivative respect to local time variance,

$$\mathbb{V}(t, \phi, \mathbf{x}) = \left. \frac{\partial \mathcal{T}(t, \tau, \phi, \mathbf{x})}{\partial \tau} \right|_{\tau=0}. \tag{8}$$

It is reasonable to match the flowmap velocity with the physical velocity at the solid boundary: $\mathbb{V}(t, \phi, \mathbf{x}) = V(t, \phi, s)$ on $\mathcal{S}$.

Meanwhile, we define a transverse map $\tilde{\mathcal{T}}$ which maps a domain with the original control ϕ to a domain with the perturbed control $\phi + \varepsilon\phi'$ at the same time moment:

$$\tilde{\mathcal{T}}(t, \varepsilon, \phi) : \Omega(t, \phi) \to \Omega(t, \phi + \varepsilon\phi'). \tag{9}$$

A transverse map velocity Z is defined accordingly respect to ε,

$$Z(t,\phi,\mathbf{x}) = \left.\frac{\partial\tilde{\mathcal{T}}(t,\varepsilon,\phi,\mathbf{x})}{\partial\varepsilon}\right|_{\varepsilon=0}. \tag{10}$$

With the help of the above toolbox from noncylindrical calculus, we can first define the perturbation derivative in Lagrangian point of view, called noncylindrical material derivative,

$$\dot{f}(t,\mathbf{x}) \equiv \lim_{\varepsilon\to 0}\frac{f(t,\phi+\varepsilon\phi',\tilde{\mathcal{T}}(t,\varepsilon,\phi,\mathbf{x})) - f(t,\phi,\mathbf{x})}{\varepsilon}, \tag{11}$$

then, the perturbation derivative in Eulerian point of view, called noncylindrical shape derivative,

$$f' = \dot{f} - Z_i\frac{\partial f}{\partial x_i}, \tag{12}$$

which can be used directly for equations presented in Eulerian framework. The transverse velocity and flowmap velocity can be related by the noncylindrical material derivative,

$$\dot{\mathbb{V}}_i = \frac{dZ_i}{dt}. \tag{13}$$

II.C. Linearized perturbation equation

The linearized perturbation equation is derived using shape derivative:

$$\begin{aligned} \mathcal{N}'(\mathbf{q})\mathbf{q}' &= \mathbf{F}' && in\ \ \Omega,\\ u_i' &= \dot{u}_i - Z_j\frac{\partial u_i}{\partial x_j} && on\ \ \mathcal{S}, \end{aligned} \tag{14}$$

where

$$\mathcal{N}'(\mathbf{q})\mathbf{q}' = \begin{bmatrix} \dfrac{\partial u_j'}{\partial x_j} \\ \dfrac{\partial u_i'}{\partial t} + \dfrac{\partial u_j' u_i}{\partial x_j} + \dfrac{\partial u_j u_i'}{\partial x_j} - \nu\dfrac{\partial^2 u_i'}{\partial x_j^2} + \dfrac{\partial p'}{\partial x_i} \end{bmatrix}, \qquad \mathbf{F}' = 0, \tag{15}$$

and $\dot{u}_i = \dot{V}_i$ corresponds to the change of boundary velocity (control) in a Lagrangian framework.

II.D. Adjoint equation

Introducing adjoint variables $\mathbf{q}^* = [p^*\ \mathbf{u}^*]^T$ as a Lagrangian multiplier for the constraint of governing equations and then apply the above definition of shape derivatives on the enhanced cost function, we have:

$$\mathcal{J}' = \int_0^T\int_{\Omega_o} 2(\mathbf{u}-\mathbf{u}_0)\cdot\mathbf{u}'d\mathbf{x}dt + \int_0^T\int_{\Omega(t)}\mathbf{q}^*\cdot[\mathcal{N}'(\mathbf{q})\mathbf{q}' - \mathbf{F}']d\mathbf{x}dt. \tag{16}$$

Integrate by part, then

$$\mathcal{J}' = b - \int_0^T\int_{\Omega(t)}\mathbf{q}'\cdot[\mathcal{N}^*(\mathbf{q})\mathbf{q}^* - \mathbf{F}^*]d\mathbf{x}dt, \tag{17}$$

where

$$\begin{aligned} \mathcal{N}^*(\mathbf{q})\mathbf{q}^* &= \begin{bmatrix} \dfrac{\partial u_j^*}{\partial x_j} \\ \dfrac{\partial u_i^*}{\partial t} + u_j\left(\dfrac{\partial u_i^*}{\partial x_j} + \dfrac{\partial u_j^*}{\partial x_i}\right) + \nu\dfrac{\partial^2 u_i^*}{\partial x_j^2} + \dfrac{\partial p^*}{\partial x_i} \end{bmatrix},\\ \mathbf{F}^* &= \begin{bmatrix} 0 \\ 2(u_i - u_{0i})\chi_o(\Omega_o) \end{bmatrix}, \end{aligned} \tag{18}$$

and χ_o is a characteristic function define as

$$\chi_o = \begin{cases} 1 & in\ \ \Omega_o \\ 0 & otherwise \end{cases}. \tag{19}$$

The boundary terms from integration by part are

$$\begin{aligned} b = & \int_{\Omega(t,\phi)} (u_j^* u_j')|_{t=0}^{t=T} d\mathbf{x} + \mathbf{B}_\infty \\ & + \int_0^T \int_{\mathcal{S}} u_i^* \left[-p' \delta_{ij} + \nu \left(\frac{\partial u'_i}{\partial x_j} + \frac{\partial u'_j}{\partial x_i} \right) \right] n_j ds dt \\ & - \int_0^T \int_{\mathcal{S}} u'_i \left[p^* n_i + u_i^* u_j n_j + u_j^* u_j n_i + \nu \left(\frac{\partial u_i^*}{\partial x_j} + \frac{\partial u_j^*}{\partial x_i} \right) n_j - u_i^* V_j n_j \right] ds dt, \end{aligned} \tag{20}$$

where $\mathbf{B}_\infty$ is the boundary term at the far-field, δ_{ij} is Kronecker's delta and n_i is the norm direction from solid to fluid. We can choose the following adjoint equation along with appropriate boundary conditions to simplify the form of $\mathcal{J}'$:

$$\begin{aligned} \mathcal{N}^*(\mathbf{q})\mathbf{q}^* = \mathbf{F}^* \qquad & in\ \ \Omega, \\ u_i^* = 0 \qquad & on\ \ \Gamma_\infty\ \&\ \mathcal{S}, \\ u_i^* = 0 \qquad & at\ \ t = T. \end{aligned} \tag{21}$$

In this way, many terms in (20) reduce to zero and the $\mathcal{J}'$ only depends on the perturbation of variables along the solid boundary.

II.E. Gradient calcuation

With adjoint equation and the boundary/initial conditions in (21), $\mathcal{J}'$ is reduced to

$$\begin{aligned} \mathcal{J}' &= -\int_0^T \int_{\mathcal{S}} u'_i \left[p^* n_i + \nu \left(\frac{\partial u_i^*}{\partial x_j} + \frac{\partial u_j^*}{\partial x_i} \right) n_j \right] ds dt \\ &= -\int_0^T \int_{\mathcal{S}} \left(\dot{V}_i - Z_k \frac{\partial u_i}{\partial x_k} \right) \left[p^* n_i + \nu \left(\frac{\partial u_i^*}{\partial x_j} + \frac{\partial u_j^*}{\partial x_i} \right) n_j \right] ds dt. \end{aligned} \tag{22}$$

The Z term can be further transferred into $\dot{V}$, which is directly related to the control. From equation (13), we have

$$\int_0^T \int_{\mathcal{S}} \dot{V}_i Z_i^* ds dt = \int_{\mathcal{S}} Z_i Z_i^* ds \Big|_0^T - \int_0^T \int_{\mathcal{S}} \left(\frac{dZ_i^*}{dt} + Z_i^* div_{\mathcal{S}} V \right) Z_i ds dt, \tag{23}$$

where the tangential divergence is defined as

$$div_{\mathcal{S}} V = \frac{\partial \mathbb{V}_i}{\partial x_i}\Big|_{\mathcal{S}} - \frac{\partial \mathbb{V}_i}{\partial x_j} n_j n_i. \tag{24}$$

Therefore let

$$\begin{aligned} Z_i^*(T) &= 0, \\ \frac{dZ_k^*}{dt} + Z_k^* div_{\mathcal{S}} V &= \frac{\partial u_i}{\partial x_k} \left[p^* n_i + \nu \left(\frac{\partial u_i^*}{\partial x_j} + \frac{\partial u_j^*}{\partial x_i} \right) n_j \right], \end{aligned} \tag{25}$$

along with the fact $Z_i(0) = 0$, $\mathcal{J}'$ can be simplified as:

$$\mathcal{J}' = -\int_0^T \int_{\mathcal{S}} \dot{V}_i \left[p^* n_i + \nu \left(\frac{\partial u_i^*}{\partial x_j} + \frac{\partial u_j^*}{\partial x_i} \right) n_j + Z_i^* \right] ds dt. \tag{26}$$

With the definition $\dot{V}_i(t, \phi', s) = \frac{\partial V_i}{\partial \phi} \phi'$, we can get the final gradient formulation. Note that the first two terms (without Z_i^*) in (26) are the same as those derived by the traditional approach for fixed domain, while the last term (with Z_i^*) is introduced by domain variation.

III. Numerical Simulation for Fluid Flow and Adjoint

Since the continuous approach is used, the above adjoint equation and formulation for gradient information is independent of numerical algorithm. For both forward (physical) simulation and backward (adjoint) simulation, we have applied different techniques for the treatment of moving boundaries: 1) immersed boundary method [21]; 2) arbitrary Lagrangian-Eulerian (ALE) method [22]; 3) for simple rigid cases, moving reference frame algorithm [23], which all produce similar results and efficiency. We used central difference for spatial discretization, third-order Runge-Kutta/Crank-Nicolson scheme for time advancement and projection method to keep the incompressible constrains [3]. The simulation result has been validated against the result in [24]. With the similarity shown in the form of adjoint equation and original flow equation, we were able to apply the numerical scheme in a very similar way to compute the adjoint solution backward in time. The computational cost is also similar between the forward and backward processes.

With the gradient calculated, the control is updated in the same way as it is in our earlier work [14]: the Polak-Ribiere variant of the conjugate gradient method is used for iterations and, within each iteration, the Brent's method is used for line minimization [25].

IV. Validation and Applications

In this section, we first validate our adjoint-based algorithm by a two-dimensional test case where a rigid plate plunges normal to the incoming flow. Then, the algorithm is applied to optimize the phase delay between plunging and pitching motion for drag reduction. Finally, we extend the approach to a three-dimensional problem with an oscillatory sphere and incoming flow.

IV.A. Validation: a plunging plate with incoming flow

The plate has length $l = 1$, which is the characteristic length for nondimensionalization, and nondimensional thickness $h = 0.04$. It is located at the center of the computational domain with $-10 < x < 10$ and $-10 < y < -10$. The grid is uniformly distributed in the vicinity of the solid plate and stretched to the far field. The Reynolds number defined by the incoming flow velocity is $Re = 100$. The control ϕ is the plunging velocity at each individual moment as shown below:

$$\begin{aligned} V_1(t) &= 0 \\ V_2(t) &= \{\phi(t_1), \phi(t_2), ..., \phi(t_n)\}. \end{aligned} \tag{27}$$

The same cost function is used as in (1). The observation region Ω_o lies one chord length behind the plate, as marked in figure 1. For validation, we first performed a simulation with a target control $\phi^{(0)}$ and recorded the velocity field $\mathbf{u}_0$ in Ω_o as our target velocity. Then, an arbitrary initial control $\phi^{(1)}$ different from $\phi^{(0)}$ was chosen with the cost function to match the target velocity. Such a setup obviously has an optimal solution $\phi^{(0)}$, which can be used to test the performance of our optimization algorithm.

The initial and target controls are given by:

$$\begin{aligned} \phi^{(0)}(t) &= 2A_0\pi k \sin(2\pi k t), \\ \phi^{(1)}(t) &= 2A_1\pi k \sin(2\pi k t), \end{aligned} \tag{28}$$

where $A_0 = 0.2$, $A_1 = 0.1$ and $k = 0.2$. Figure 1 shows the flow field and adjoint field. The adjoint information/variable can originate from the adjoint boundary condition, the term $u_j(\partial u_j^*/\partial x_i)$, and the right-hand-side source term $\mathbf{F}^*$. In the current case, homogeneous boundary condition is used, thus the adjoint field can be only generated from the last two terms. Figure 1 (c-f) show the development of the adjoint velocity when it evolves backward in time. First, the adjoint field originates from the area Ω_o due to the term $\mathbf{F}^*$. There is some concentration of adjoint energy caused by the term $u_j(\partial u_j^*/\partial x_i)$. The whole adjoint field convects upstream at speed u_i when evolving backward in time. When it reaches the plate, there are noticeable beam-shape structures. After passing by the plate, the adjoint field continues convecting upstream and is eventually dissipated due to the dissipation term in the adjoint equation.

To validate the gradient calculation, we compare the gradients obtained from our adjoint approach and from finite difference approach. The finite difference approach is to perturb the control and calculate the gradient g directly from (2). In our case, the perturbation of the control at time t_l can effect the cost

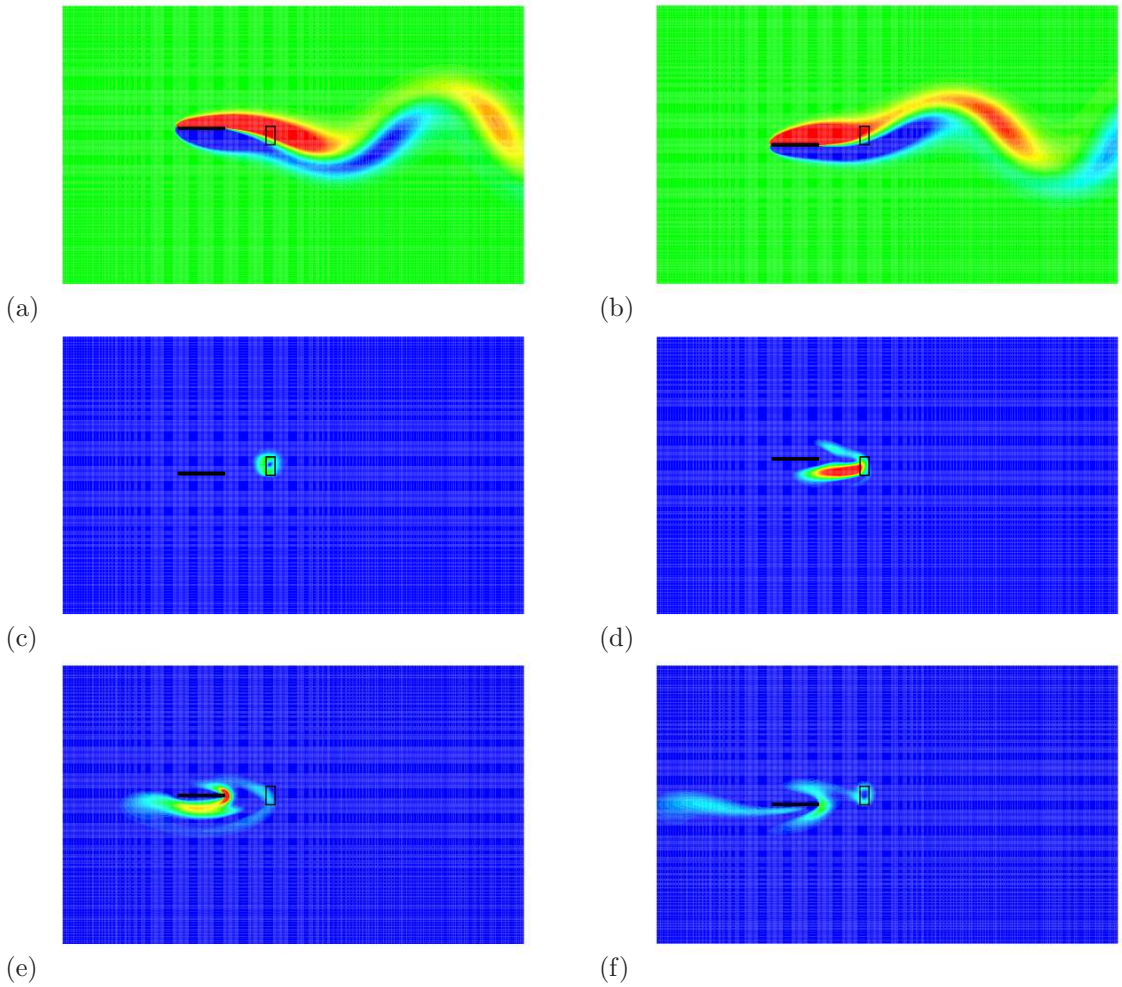

Figure 1. The forward flow field of vortex at different time (a,b); The adjoint flow field of velocity magnitude at (c) $t = 9.75$, (d) $t = 9$, (e) $t = 8.125$ and (f) $t = 7.375$.

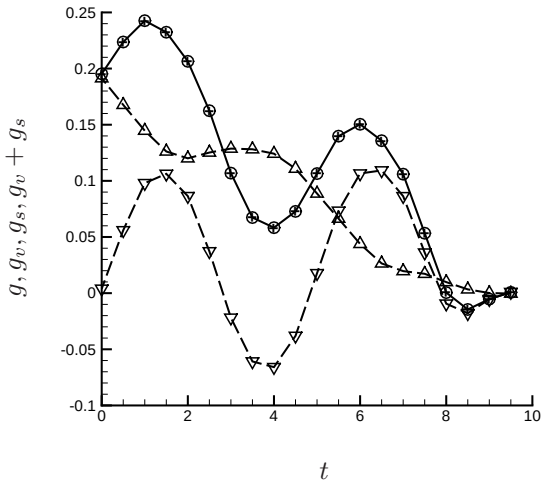

Figure 2. The gradient g ($\circ$), g_v (∇), g_s ($\triangle$) and $g_v + g_s$ ($+$) calculated from finite difference approach.

function and eventually the gradient in two ways: the perturbation of the instant boundary velocity and the perturbation of the plate location at the later time, which can be written as:

$$\delta V_i = \begin{cases} \delta\phi(t_l) & i = 2 \;\&\; t = t_l \\ 0 & otherwise \end{cases}, \qquad \delta S_i = \begin{cases} \delta\phi(t_l)\Delta t & i = 2 \;\&\; t > t_l \\ 0 & otherwise \end{cases}. \tag{29}$$

These two types of perturbation are decoupled and considered separately. First, we perturb the velocity of the solid boundary without changing its future location, and use (2) to calculate the gradient due to the boundary velocity perturbation, g_v; then, we perturb the boundary location without changing its velocity and calculate the gradient due to the boundary location perturbation g_s. Figure 2 shows that these two gradients can be linearly superposed:

$$g = g_v + g_s, \tag{30}$$

when perturbations are small. In fact, the gradient due to the boundary location perturbation corresponds to the term involving Z_i^* in (26), while the gradient due to the boundary velocity perturbation corresponds to the remaining terms:

$$\begin{aligned} g_v(t) &= -\int_{\mathcal{S}} \left[p^* n_2 + \nu \left(\frac{\partial u_2^*}{\partial x_j} + \frac{\partial u_j^*}{\partial x_2} \right) n_j \right] ds, \\ g_s(t) &= -\int_{\mathcal{S}} Z_2^* ds. \end{aligned} \tag{31}$$

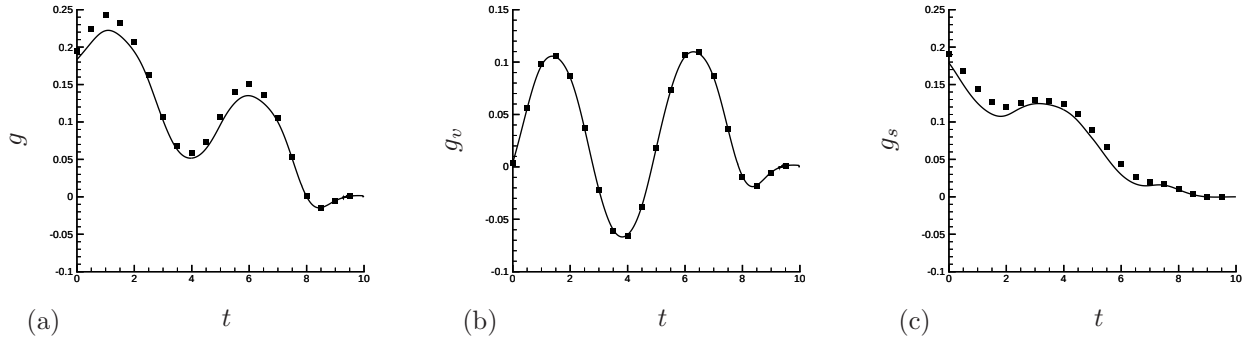

Figure 3. Comparison of different components and the total gradient g between the values computed by the adjoint method (———) and the finite difference approach through direct perturbation (■): (a) total gradient g; (b) component g_v; (c) component g_s.

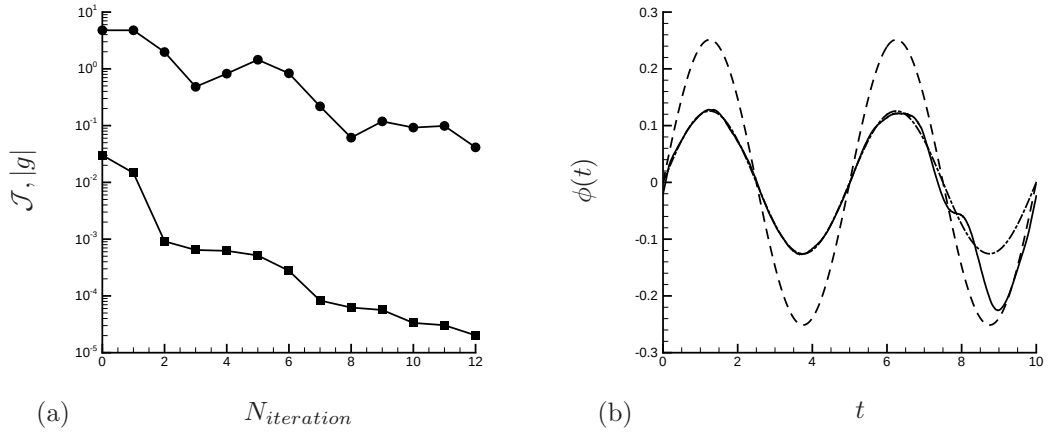

Figure 4. Optimization outcomes for the validation case: (a) eeduction of cost function (■) and the norm of the gradient (•) along with iteration numbers; (b) comparison of the target control $\phi^{(0)}$ (-·-·-), initial control $\phi^{(1)}$ (- - - -) and optimal control $\phi^{(p)}$ (———).

Figure 3 shows a good agreement between the gradients calculated by the adjoint method and the finite difference approach. The gradient g_v from the two methods matches exactly with each other, while there is only small discrepancy for the gradient g_s.

With 12 main iterations, the adjoint optimization reduces the cost function by 3 orders and the gradient norm by 2 orders, as seen in figure 4. The control is changed from $\phi^{(1)}$ to $\phi^{(p)}$. The optimized control $\phi^{(p)}$ is very close to the target control $\phi^{(0)}$ for $t < 8$. Difference between $\phi^{(0)}$ and $\phi^{(p)}$ happens after $t = 8$. This is because the information of the plate's plunging motion has not been fully transferred downstream to the observation region yet. From the view of the adjoint field, the adjoint information has not fully reached the plate yet for $t > 8$.

IV.B. Optimization on the drag reduction of a plunging and pitching plate

In this section, we apply our new adjoint approach on the pitching and plunging plate with incoming flow. Following [26], the plate oscillates vertically and pitches about a point O at one third chord length from the leading-edge, as shown in figure 5. The motion is defined by:

$$\begin{aligned} y(t) &= y_0 \sin(2\pi k t), \\ \theta(t) &= \theta_0 \sin[2\pi k t + \varphi(t)], \end{aligned} \tag{32}$$

where $k = 0.2$, $y_0 = 0.75$ and $\theta_0 = 27.2°$. The Reynolds number is 300.

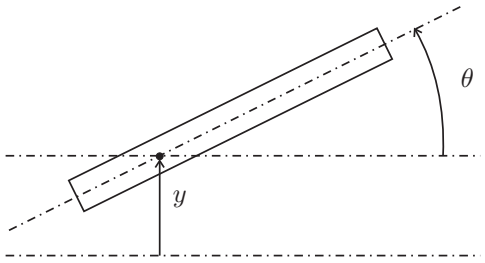

Figure 5. The sketch of the pitching and plunging motion of plate. The incoming flow comes from left to right.

As discussed in [26], the phase delay between the pitching and plunging motions is critical to thrust producing and propulsive efficiency. For this reason, we also choose the phase delay as the control: $\phi(t) = \varphi(t)$, and apply the adjoint approach to optimize it for drag reduction. The phase delay is optimized by two-steps. First, we consider the delay being a constant in time and find out its optimal value. After the optimal constant is achieved, we use it as the initial condition to optimize it further as a function of time. The two-step strategy brings the control to a good neighborhood in a simple control space (constant delay) before it becomes a complex control space (time-varying delay). Here, only periodic motion is considered. After the transition stage, the flow field is forced to be periodic. The periodicity is also reenforced in the calculation of the gradient.

To reduce the drag, we define the cost function as:

$$\mathcal{J} = \frac{2}{\rho U^2 T} \int_0^T \int_{\mathcal{S}} \sigma_{1j} n_j ds dt, \tag{33}$$

where $\sigma_{ij} = -p\delta_{ij} + \nu \left(\frac{\partial u_i}{\partial x_j} + \frac{\partial u_j}{\partial x_i} \right)$. Following similar steps before, we can get the perturbed cost function,

$$\mathcal{J}' = \frac{2}{\rho U^2 T} \int_0^T \int_{\mathcal{S}} \left(\sigma'_{1j} n_j + \frac{\partial \sigma_{1j}}{\partial x_j} Z_k n_k \right) ds dt. \tag{34}$$

Set boundary conditions,

$$\begin{aligned} \mathbf{F}^* &= 0 \qquad\quad in\ \ \Omega, \\ u_i^* &= -\delta_{1i} \qquad on\ \ \mathcal{S}, \end{aligned} \tag{35}$$

and let

$$Z_i^* = \sigma_{ij}^* n_j + u_j^* u_j n_i \qquad on\ \ \mathcal{S}, \tag{36}$$

where $\sigma^*_{ij} = p^*\delta_{ij} + \nu\left(\frac{\partial u^*_i}{\partial x_j} + \frac{\partial u^*_j}{\partial x_i}\right)$, we can get gradient,

$$g(t) = \frac{2}{\rho U^2 T}\int_{\mathcal{S}} Z_k\left(\frac{dZ^*_k}{dt} + Z^*_k div_{\mathcal{S}} V + Z^*_i\frac{\partial u_i}{\partial x_k} + \frac{\partial \sigma_{1j}}{\partial x_j}n_k\right)ds. \tag{37}$$

IV.B.1. Control of constant phase delay

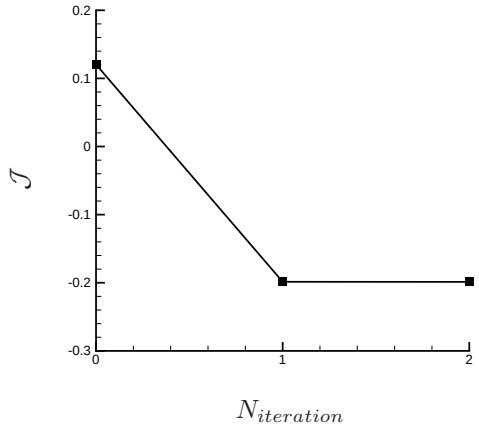

Figure 6. The reduction of drag along with iteration numbers.

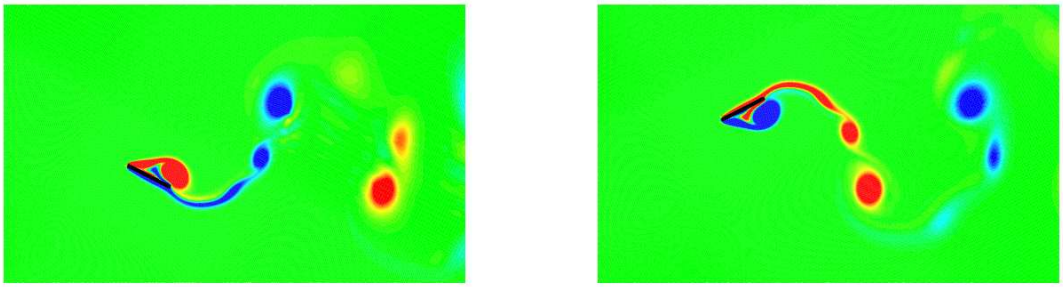

(a) (b)

Figure 7. The vortex structure for flapping plate with initial control at $\phi(t) = -30°$ during (a) upstroke and (b) downstroke.

For the constant phase delay optimization, we starts with an arbitrary initial guess for the control: $\phi^{(1)}(t) = -30°$. By 2 iterations, the control is changed to $-77.3°$ and the drag coefficient is reduced from 0.120 to -0.199 as seen in figure 6. Figure 7 and 8 compare the flow field with the initial and optimized control. For the initial control, the leading-edge vortex appears at the backside of the plate. This leading-edge vortex forms a low pressure region, thus generating drag. For the optimized control, there is no leading-edge vortex present and thrust-generating $2P$ patten vortex structure [27] can be found in the wake.

The drag reduction can also be explained by the quasi-steady model [5, 28, 29]. According to the model, the lift-based thrust is a product of plunging velocity and circulation along the plate. In current configuration, positive thrust can be generated when the plate flaps upward with anti-clockwise circulation or downward with clockwise circulation, otherwise negative thrust (drag) is produced. Shown in the flow with initial control (figure 7), a strong leading-edge vortex implying strong clockwise circulation is observed during the upstroke and the anti-clockwise circulation is observed during the downstroke. They both contribute to large drag force. On the other hand, shown in the flow with optimal control (figure 8), the absence of such leading-edge vortices suggests the reduction of drag-producing circulation, thus, less drag is experienced.

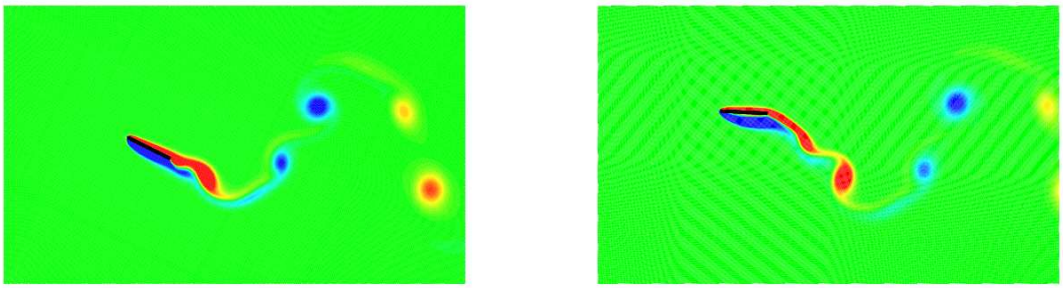

(a) (b)

Figure 8. The vortex structure for flapping plate with optimal constant phase delay during (a) upstroke and (b) downstroke.

IV.B.2. Control of time-varying phase delay

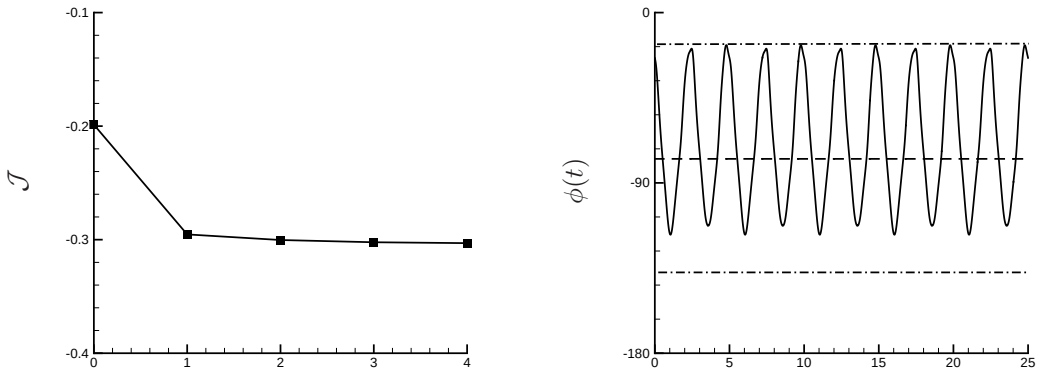

(a) (b)

Figure 9. Optimization outcome of drag reduction of a two-dimensional flapping plate: (a) reduction of the cost along with iterations; (b) the initial (– – – –) and optimal (———) phase delay for the time-varying phase optimization. The dash-dot lines (–·–·–) represent the upper and lower limits for the control.

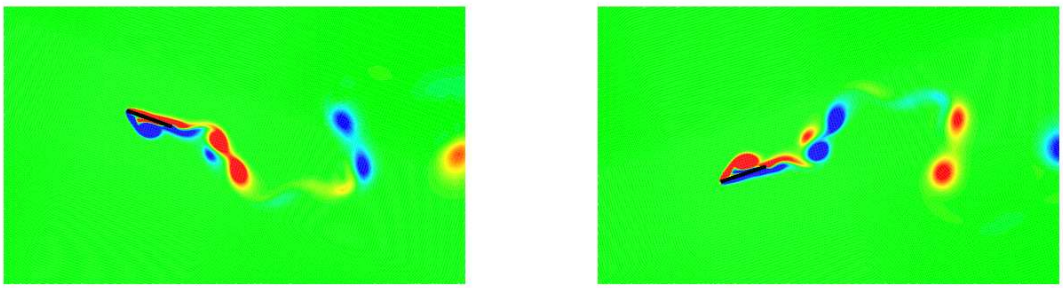

(a) (b)

Figure 10. The vortex structure for flapping plate with optimal time-varying phase delay during (a) upstroke and (b) downstroke.

For the time-varying phase delay optimization, we starts the initial control with the optimal constant phase delay: $\phi^{(1)}(t) = -77.3°$. In order to avoid very wild variation for optimization result, we put a constraint condition on the control:

$$\phi^{(1)} - \Delta\phi \leq \phi(t) \leq \phi^{(1)} + \Delta\phi, \tag{38}$$

where $\Delta\phi = 60°$. This constraint is carried out by adding a penalty term into the cost function. The

modified cost function is

$$\tilde{\mathcal{J}} = \mathcal{J} + \int_0^T \Theta\left(\frac{\phi(t) - \phi^{(1)}}{\Delta\phi}\right) dt, \tag{39}$$

where Θ is the penalty function, defined by

$$\Theta(x) = \begin{cases} \beta(x-1)^4 & x > 1 \\ 0 & -1 \le x \le 1 \\ \beta(x+1)^4 & x < -1 \end{cases}. \tag{40}$$

The penalty function is chosen in such way that it allows continuity at least for the first order derivative. The parameter β is a large positive number, which controls the strength of the penalty. The gradient is changed accordingly with the added penalty.

With 4 iterations, the optimization algorithm reduces the drag from -0.198 to -0.303 with a reduction at 53%. The optimized phase-delay varies with the frequency of drag F_x at $2k$. It reaches the upper limit of the constraint. If the constraint condition is loosen, the optimization approach can reduce the drag further.

Figure 10 shows the vortex structure under the optimal control. The time-varying phase delay changes the instant angle of attack. The strong leading-edge vortex, instead of being removed in the optimal constant-phase-delay case, is moved forward to the front side of the plate. Therefore, the new location of leading-edge vortices generate large thrust in both upstroke and downstroke.

IV.C. Optimization on oscillatory sphere

The optimization algorithm can be easily extended to three dimension. In this section, we use the adjoint approach to optimize the motion of an three dimensional sphere which oscillates vertically across the coming flow. The control, cost function and other parameters are all same as those for the two-dimensional plunging plate in section IV.A. The only difference is that we only consider periodic state here.

Figure 11 shows that the cost function is reduced by about 3 orders after 5 main iterations. The control is optimized from $\phi^{(1)}$ to $\phi^{(p)}$, very close to the target control $\phi^{(0)}$. The perfect matching between $\phi^{(p)}$ and $\phi^{(0)}$ confirms that the discrepancy in section IV.A is caused by the physical transition rather than the optimization algorithm.

Figure 12 and 13 show the vortex topology and the adjoint field for oscillatory sphere. Similar to the plunging plate, the adjoint field originates from the observation region and convects to the upstream when evolving backward in time. After passing by the sphere, the adjoint field is gradually damped out due to the dissipation.

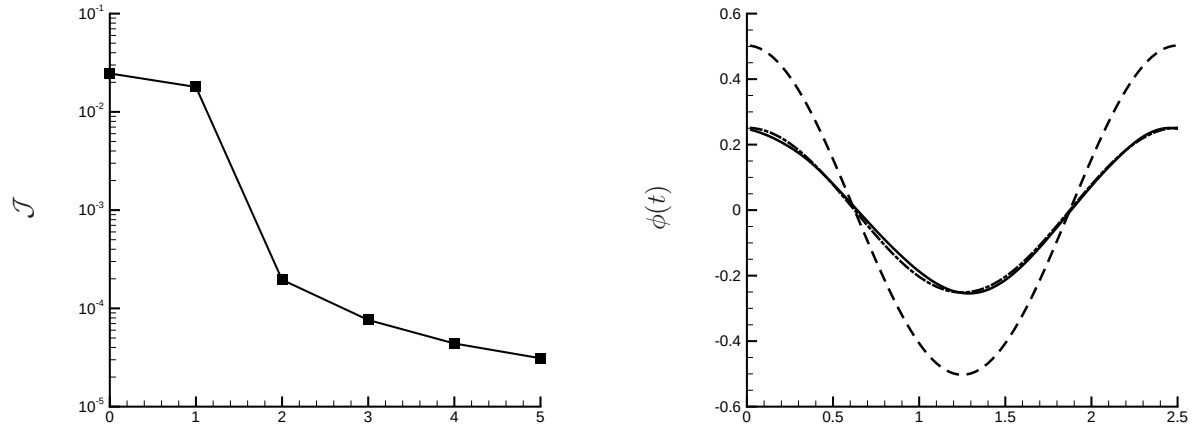

Figure 11. Optimization outcome of a three-dimensional sphere oscillation with incoming flow: (a) reduction of cost function along with iteration numbers; (b) comparison of the target control $\phi^{(0)}$ (-·-·-), initial control $\phi^{(1)}$ (- - - -) and optimal control $\phi^{(p)}$ (———).

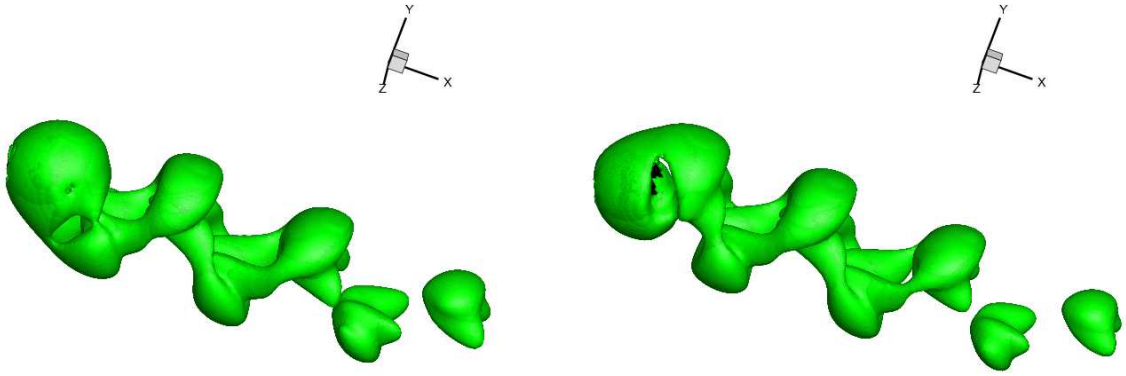

(a) (b)

Figure 12. The iso-surfaces of the Q-criterion for the flow field of the oscillatory sphere at different times.

(a) (b)

Figure 13. The iso-surfaces of the adjoint velocity norm for the adjoint flow field of the oscillatory sphere at different times.

V. Conclusions

Based on non-cylindrical calculus, we are able to derive a simple formulation (with the same mathematical rigorousness) using the adjoint-based approach for the optimization problems with moving boundary/morphing domain, which are previously too complex to derive from traditional unsteady domain mapping. The continuous adjoint formulation is used to allow different numerical implementations such as immersed boundary method and arbitrary Lagrangian-Eulerian method which have all been tested.

For the test case of a plunging plate, our current approach has been benchmarked by the comparison of the gradient computed from the adjoint-based method and the one computed by finite difference through direct perturbation (with much higher computational cost). Then we apply the approach to more practical two-dimensional and three-dimensional applications. For the drag reduction of a rigid flapping plate, we optimized the phase delay between the plunging and pitching motion both as a constant (single parameter) and a time-varying function (multi parameters). The algorithm works well for both cases. The comparison between the flow field by initial control and optimal control indeed help understanding of drag reduction mechanism. The method was then applied to an oscillatory sphere with incoming flow and achieved the same success.

Acknowledgments

The authors gratefully acknowledge the support from Air Force Office of Scientific Research (AFOSR) under FA9550-12-1-0071.

References

[1]Dong, H., Mittal, R., and Najjar, F., "Wake topology and hydrodynamic performance of low aspect-ratio flapping foils," *J. Fluid Mech.*, Vol. 566, 2006, pp. 309–343.

[2]Dong, H. and Liang, Z., "The wing kinematics effects on performance and wake structure produced by finite-span hovering wings," *AIAA Paper* 2008-3819, 2008.

[3]Yang, T., Wei, M., and Zhao, H., "Numerical study of flexible flapping wing propulsion," *AIAA J.*, Vol. 48, No. 12, 2010, pp. 2909–2915.

[4]Yin, B. and Luo, H., "Effect of wing inertia on hovering performance of flexible flapping wings," *Phys. Fluids*, Vol. 22, 2010, pp. 111902.

[5]Berman, G. J. and Wang, Z. J., "Energy-minimizing kinematics in hovering insect flight," *J. Fluid Mech.*, Vol. 582, No. 1, 2007, pp. 153–168.

[6]Ghommem, M., Hajj, M. R., Mook, D. T., Stanford, B. K., Beran, P. S., Snyder, R. D., and Watson, L. T., "Global optimization of actively morphing flapping wings," *Journal of Fluids and Structures*, Vol. 33, 2012, pp. 210–228.

[7]Milano, M. and Gharib, M., "Uncovering the physics of flapping flat plates with artificial evolution," *J. Fluid Mech.*, Vol. 534, No. 1, 2005, pp. 403–409.

[8]Tuncer, I. H. and Kaya, M., "Optimization of flapping airfoils for maximum thrust and propulsive efficiency," *AIAA J.*, Vol. 43, No. 11, 2005, pp. 2329–2336.

[9]Culbreth, M., Allaneau, Y., and Jameson, A., "High-fidelity optimization of flapping airfoils and wings," *AIAA Paper* 2011-3521, 2011.

[10]Nadarajah, S. K. and Jameson, A., "Optimum Shape Design for Unsteady Flows with Time-Accurate Continuous and Discrete Adjoint Method," *AIAA J.*, Vol. 45, No. 7, 2007, pp. 1478–1491.

[11]Moubachir, M., *Moving Shape Analysis and Control: Applications to Fluid Structure Interactions*, CRC Press, Abingdon, 2006.

[12]Protas, B. and Liao, W., "Adjoint-based optimization of PDEs in moving domains," *J. Comput. Phys.*, Vol. 227, No. 4, 2008, pp. 2707–2723.

[13]Bewley, T. R., Moin, P., and Temam, R., "DNS-based predictive control of turbulence: an optimal benchmark for feedback algorithms," *J. Fluid Mech.*, Vol. 447, 2001, pp. 179–225.

[14]Wei, M. and Freund, J. B., "A noise-controlled free shear flow," *J. Fluid Mech.*, Vol. 546, 2006, pp. 123–152.

[15]Jones, M. and Yamaleev, N. K., "Adjoint-based shape and kinematics optimization of flapping wing propulsive efficiency," *AIAA Paper* 2013-2472, 2013.

[16]Lee, B. J., Padulo, M., and Liou, M.-S., "Non-sinusoidal trajectory optimization of flapping airfoil using unsteady adjoint approach," *AIAA Paper* 2011-1312, 2011.

[17]Nadarajah, S. and Jameson, A., "A comparison of the continuous and discrete adjoint approach to automatic aerodynamic optimization," *AIAA Paper* 2000-667, 2000.

[18]Giles, M. B. and Pierce, N. A., "An introduction to the adjoint approach to design," *Flow, turbulence and combustion*, Vol. 65, No. 3-4, 2000, pp. 393–415.

[19]Wang, Q. and Gao, J., "The drag-adjoint field of a circular cylinder wake at Reynolds numbers 20, 100 and 500," *J. Fluid Mech.*, Vol. 730, 2013, pp. 145–161.

[20]Xu, M. and Wei, M., "Using adjoint-based approach to study flapping wings," 51st AIAA Aerospace Sciences Meeting and Exhibit, Grapevine, TX, *AIAA Paper* 2013-839, 2013.

[21]Mittal, R., Dong, H., Bozkurttas, M., Najjar, F., Vargas, A., and Von Loebbecke, A., "A versatile sharp interface immersed boundary method for incompressible flows with complex boundaries," *J. Comput. Phys.*, Vol. 227, No. 10, 2008, pp. 4825–4852.

[22]Hirt, C., Amsden, A. A., and Cook, J., "An arbitrary Lagrangian-Eulerian computing method for all flow speeds," *J. Comput. Phys.*, Vol. 14, No. 3, 1974, pp. 227–253.

[23]Li, L., Sherwin, S., and Bearman, P. W., "A moving frame of reference algorithm for fluid/structure interaction of rotating and translating bodies," *International Journal for Numerical Methods in Fluids*, Vol. 38, No. 2, 2002, pp. 187–206.

[24]Guilmineau, E. and Queutey, P., "A numerical simulation of vortex shedding from an oscillating circular cylinder," *Journal of Fluids and Structures*, Vol. 16, No. 6, 2002, pp. 773–794.

[25]Press, W. H., Flannery, B. P., Teukolsky, S. A., and Vetterling, W. T., *Numerical Recipes*, Cambridge, 1986.

[26]Anderson, J. M., Streitlien, K., Barrett, D. S., and Triantafyllou, M. S., "Oscillating foils of high propulsive efficiency," *J. Fluid Mech.*, Vol. 360, 1998, pp. 41–72.

[27]Williamson, C. H. K. and Roshko, A., "Vortex formation in the wake of an oscillating cylinder," *Journal of Fluids and Structure*, Vol. 2, 1988, pp. 355–381.

[28]Andersen, A., Pesavento, U., and Wang, Z., "Unsteady aerodynamics of fluttering and tumbling plates," *J. Fluid Mech.*, Vol. 541, 2005, pp. 65–90.

[29]Pesavento, U. and Wang, Z. J., "Falling paper: Navier-Stokes solutions, model of fluid forces, and center of mass elevation," *Phys. Rev. Lett.*, Vol. 93, No. 14, 2004, pp. 144501.